Numerical Prediction of Flow Patterns in Bubble Pumps

Ali Benhmidene[1(*)], Bechir Chaouachi[1], Mahmoud Bourouis[2], Slimane Gabsi[1]

[1] Research Unit Environment, Catalysis and Process Analysis URECAP. The National School of Engineering of Gabès, Omar Ibn El Khattab Street, Gabes 6029, Tunisia

[2]Department of Mechanical Engineering, Universitat Rovira i Virgili, Av. Països Catalans, 26, 43007 Tarragona, Spain

(*) aahmiden@yahoo.fr, bechir.chaouachi@enig.rnu.tn, mahmoud.bourouis@urv.cat, slimane.gabsi@isetsf.rnu.tn,

Abstract

In the present study, the ammonia-water mixing flow in a bubble pump is numerically simulated. The flow patterns of a two-phase flow in a bubble pump were studied under different conditions of heat flux and tube diameter. A one-dimensional two-fluid model was developed under constant heat flux. This model was used to predict the variations of void fraction, liquid and vapor velocities throughout the tube. Then, the void fraction profile and the curve of liquid velocity versus vapor velocity were used to predict the flow patterns along the tube length. It was found that at heat fluxes below 15 $kW.m^{-2}$ bubbly, slug and churn flows are the dominating regimes, and the length of these flow regimes depends on the tube diameter. For heat fluxes higher than 15 $kW.m^{-2}$, the bubble pump operates under the churn and annular regimes, and the bubble pump performance is improved when the tube diameter increases.

Key words: bubble pump, flow pattern, void fraction, simulation

1 Introduction

A bubble pump is simply a vertical tube into which the liquid and vapor streams, coming from the boiler or generator, enter at the lower end. The liquid fills the lift tube to a designed depth. The vapor traveling upwards through this section forms bubbles that act like pistons and drive liquid slugs up the remainder of the tube.

The experiments and theoretical considerations showed that, for a specific heat input, the diameter of the lift tube has no effect on the pumping rate if the pump is running in the slug or churn flow regimes [1-3]. When the maximum lift-tube diameter is exceeded, the flow pattern changes from slug flow to an intermittent churn-type flow [4,5]. The bubble pump model presented by Delano [6] assumed that all flow takes place in the slug flow regime. At first, it may seem that a pump tube with a larger diameter would always be advantageous. However, increasing the diameter when the liquid flow is constant will eventually cause the assumed slug flow to change to bubbly flow. White [7] showed a rapid decrease in efficiency when the diameter drops below a particular value. This rapid decrease is due to the transition from slug to churn flow.

According to what has been reported above, the studies available in the open literature on flow patterns in a bubble pump are mainly based on experimental measurements. These studies showed that the bubble pump is more efficient when operating under the slug flow regime [7, 8]. The flow pattern prediction of flow boiling in a bubble pump has not been deeply studied in the literature. Chilshom's correlation

[9] (Eq. 1) is usually used to calculate the tube diameter of the bubble pump. This correlation, which calculates the maximum tube diameter for which the slug flow regime occurs [10], has the disadvantage that requires the existence of a single flow regime along the tube. However, in a bubble pump several flow regimes can coexist.

$$D \leq \left(\frac{\sigma . \rho_f}{g\left(1 - \frac{\rho_f}{\rho_g}\right)} \right) \tag{1}$$

Regarding the regime transition in a bubble pump, White [7] used the equation of Hewitt and Wallis [11] to predict the regime transition from slug to semi-annular flow. But, there is very scarce information on the regime transition in a bubble pump from bubbly to slug flow or from semi-annular to annular flow. Moreover, the effect of heat flux received by the bubble pump on the flow pattern has not been studied.

On the other hand, flow pattern can be predicted using other criteria such as the void fraction profile. Radovich and Moissis [12] considered individual bubble fluctuations within a cubic lattice structure and determined a relation between frequency of bubble collision and void fraction that indicated that the collision frequency was very high at a void fraction of 0.3. The transition from bubbly to slug flow occurs at the void fraction around 0.3 [13, 14]. Also, according to experimental data, when the void fraction is less than 0.2 transition to slug regime is rarely occurs and the fraction is seldom more than 0.3 [14].

Barnea and Brauner [16] considered that the formation of highly aerated liquid slugs was the reason for transition from slug flow to churn flow. When the void fraction in the liquid slugs reaches 0.52, the separation between bubbles is too small and collision and coalescence cannot be avoided.

In annular flow, decreasing the vapor flow rate reduces the void fraction, and if it becomes critical liquid bridges may be formed by the crests of interfacial waves. Under this condition, the transition from annular flow to intermittent (churns or slug) flow takes place. By comparing void fraction data with theoretical predictions for annular flow and intermittent flow, Wallis [17] obtained a critical void fraction of 0.80. Barnea [18] suggested that when the void fraction is lower than 0.76, annular flow will change to intermittent flow because of the liquid blockage. Haberstroh and Griffith [19] studied slug-annular transition in various fluid systems and with several tube diameters. They found that transition occurred at a void fraction of between 0.80 and 0.90.

In the present study, the bubble pump was a vertical uniformly heated tube that operates at high pressure (P = 18 bar) with ammonia-water mixture. Flow patterns were simulated for operating conditions involving different heat fluxes and different tube diameters. They were predicted by void fraction profiles and liquid velocity curves versus vapor velocity curves.

2 Mathematical Model

Most of the models reported in the literature for two-phase flow in a bubble pump use Beattie and Whalley's method [20] and the drift flux method (Zuber and Findlay [21]) to calculate the two-phase friction factor and the gas void fraction, respectively. The difference between these models is the value of the coefficients used in the drift flux model.

In the recent decades, significant developments in the two-phase flow formulation have been accomplished by introducing and improving the two-fluid model. The two-fluid model can be considered the most detailed and accurate macroscopic formulation of the thermo-fluid dynamics of two-phase flow [22-24]. This model treats the general case of modeling each phase or component as a separate fluid with its own set of governing balance equations.

In the present work, the two-fluid model is used to predict the void fraction profile and the superficial velocity in each phase. This model considers non-equilibrium hydrodynamic conditions.

2.1 The Two-Fluid Model. In the two-phase region, the general conservation equations of mass, momentum and energy were formulated by Ishii and Mishima [25]. For the steady state with negligible kinetic and potential energy, the conservation equations are reduced to the following five equations:

- Phase mass equations

$$\frac{d}{dz}\left(\alpha\rho_G u_G\right) = \Gamma_G \tag{2}$$

$$\frac{d}{dz}\left[\left(1-\alpha\right)\rho_L u_L\right] = \Gamma_L \tag{3}$$

- Phase momentum equations

$$\frac{d}{dz}\left(\alpha\rho_G u_G^2\right)+\alpha\frac{dP}{dz}+\alpha\rho_G g=-F_{WL}-F_{GL}-F_{GI} \tag{4}$$

$$\frac{d}{dz}\left((1-\alpha)\rho_L u_L^2\right)+(1-\alpha)\frac{dP}{dz}+(1-\alpha)\rho_L g=-F_{WL}+F_{LG}-F_{LI} \tag{5}$$

- Mixture energy equation

$$\frac{d}{dz}\left[(1-\alpha)\rho_L u_L H_L+\alpha\rho u_G H_G\right]=\frac{q_w P_h}{A} \tag{6}$$

2.2 Interfacial Momentum Transfer. The drag force; F_{LG} is modeled according to Richter [26]:

$$F_{LG}=\frac{3C_{FI}}{D}\sqrt{\alpha}\rho_G(u_G-u_L)|u_G-u_L|+C\rho_G u_G\alpha\frac{d}{dz}(u_G-u_L) \tag{7}$$

C' is a virtual mass coefficient taken as:

- C' = 0.5 for bubbly flow
- C' = 0 for other flow regimes.

The interfacial friction factor C_{FI} is taken as

$$\begin{cases} C_{FI}=C_D\sqrt{\alpha}\,(1-\alpha)^{-1.7}\,\dfrac{\rho_L}{\rho_G}\dfrac{D}{D_B} \\ \text{for bubbly flow} \\ C_{FI}=0.005\left(1+75(1-\alpha)\right) \\ \text{for annular flow} \end{cases} \tag{8}$$

In the intermediate flow regimes with a medium void fraction between the bubbly and annular flow, C_{FI} is interpolated linearly with the void fraction between the two values given in Eq. (8).

The drag coefficient for a single bubble C_D in Eq. (8) depends on the bubble Reynolds number Re_B:

$$C_D = \frac{24}{\mathrm{Re}_B}\left(1+0.15\,\mathrm{Re}_B^{0.687}\right) \qquad \mathrm{Re}_B < 1000$$

$$C_D = 0.44 \quad \mathrm{Re}_B \geq 1000$$

where

$$\mathrm{Re}_B = \frac{2\rho_L R_B (1-\alpha)|u_G - u_L|}{\mu_L}$$

The interfacial momentum transfers F_{GI} and F_{LI} caused by the mass transfer can be determined from Eq. (4) and (5) while the liquid evaporates. The force associated with this velocity change is described by the following terms:

$$F_{LI} = -(1-\eta)\Gamma_L (u_L - u_G) \tag{9}$$

$$F_{GI} = -\eta\Gamma_G (u_G - u_L) \tag{10}$$

Where η is the phase distribution factor, η = 0.5 for bubbly flow and η = 0 in the other flow regime [27].

The wall-liquid friction F_{WL} is modeled by Chisholm's correlation [28] because it fits Baroczy's advanced empirical correlation curves [29] quite well and takes into account the effect of mass flux on the friction pressure gradient. The correlation is expressed by the following set of equations:

$$F_{WL} = \left(1+\left(Y^2-1\right)\left(Bx^{(2-n)/2}(1-x)^{(2-n)/2} + x^{2-n}\right)\right)\Delta P_{Lo} \tag{11}$$

Where ΔP_{Lo} is the single-phase friction pressure drop that would exist if the total mass flow of the two-phase mixture flowed as a single liquid phase. It is given by:

$$\Delta P_{Lo} = \frac{4}{D} f_{Lo} \frac{G^2}{2\rho_L} \tag{12}$$

n = 0.25 for the Blasius equation.

$$Y = \left(\frac{\Delta P_{Go}}{\Delta P_{Lo}} \right)^{0.5} = \left(\frac{f_{Go}}{f_{Lo}} \right)^{0.5} \tag{13}$$

Coefficient B in Eq. (11) is denoted as:

$$B = \frac{CY - 2^{2-n} + 2}{Y^2 - 1} \tag{14}$$

$$\text{Where} \quad C = \frac{u_G}{u_L} \sqrt{\frac{\rho_L}{\rho_G}} \left(1 + \frac{u_G^2}{u_L^2} \frac{\rho_G}{\rho_L} \right) \tag{15}$$

And the true vapor mass quality is expressed as:

$$x = \frac{1}{1 + \frac{1-\alpha}{\alpha} \frac{\rho_L}{\rho_G} \frac{u_L}{u_G}} \tag{16}$$

2.3 Vapor Generation Rate. The heat transfer rate q_e due to evaporation can be modeled by the following equation:

$$q_e = C_2 \left(q_w - C_1 h_{sp} \left(T_w - T_L \right) \right) \tag{17}$$

C_1 and C_2 were estimated by Hainoun et al. [30]:

$$\begin{aligned} C_1 &= 1 - \frac{\pi}{16} \frac{\alpha}{\alpha_{OSV}} \ for \ \alpha \le \frac{16.\alpha_{OSV}}{\pi} \\ C_1 &= 0 \ for \ \alpha \succ \frac{16.\alpha_{OSV}}{\pi} \end{aligned} \tag{18}$$

$$C_2 = \left(\frac{T_w - T_{sat}}{T_w - T_L} \right)^2 \tag{19}$$

h_{sp} is the single liquid phase heat transfer coefficient given by:

$$h_{sp} = 0.023 \frac{\lambda_L}{D} \mathrm{Re}_L^{\ 0.8} \, \mathrm{Pr}_L^{\ 0.4} \tag{20}$$

Re_L is the Reynolds number in the liquid phase expressed by:

$$\mathrm{Re}_L = \frac{GD(1-x)}{\mu_L} \tag{21}$$

The wall temperature T_w is calculated from:

$$q_w = h_{tp}\left(T_w - T_L\right) \tag{22}$$

The method for expressing the forced convection boiling heat transfer coefficient h_{tp} is derived from Chen's well-known correlation [31]. This method was used by Celata et al. [32] to predict the convective boiling heat transfer coefficient for R12/R114 binary mixtures. The convective boiling heat transfer coefficient can be expressed as the arithmetic summation of the two-phase convection contribution h_{cv} and the boiling contribution h_{nb}:

$$\begin{aligned} h_{tp} &= h_{cv} + h_{nb} \\ h_{cv} &= Fh_{sp} \quad \text{et} \quad h_{nb} = Sh_{npb} \end{aligned} \tag{23}$$

The factor F represents the acceleration effect of liquid due to vapor shear stress. The pool boiling heat transfer coefficient h_{npb} is computed for the same value of wall super heat as for forced convective boiling. The factor S represents the suppression of nucleate boiling due to the liquid flow.

Several correlations have been proposed for calculating F, S and h_{npb}. In this paper we have used Chen's correlation [31]:

$$\begin{aligned} F &= 1 \quad \text{for} \quad \frac{1}{\mathrm{Xtt}} \le 0.1 \\ F &= 2.35\left(\frac{1}{Xtt} - 0.213\right)^{0.736} \quad \text{for} \quad \frac{1}{Xtt} \succ 0.1 \end{aligned} \tag{24}$$

The Lockhart-Martinelli parameter is expressed by:

$$\frac{1}{Xtt} = \left(\frac{\rho_L}{\rho_g}\right)^{0.5}\left(\frac{\mu_g}{\mu_L}\right)^{0.1}\left(\frac{x}{1-x}\right)^{0.9} \tag{25}$$

$$S = \left(1 + 2.35.10^{-6}\,\mathrm{Re}_{tp}^{\,1.17}\right)^{-1} \tag{26}$$

$$h_{npb} = 0.00122\left(\frac{\mu_L^{\,0.79} Cp_L^{\,0.45} \rho_L^{\,0.49}}{\sigma^{0.5} \mu_L^{\,0.29} h_{fg}^{\,0.24} \rho_g^{\,0.24}}\right) \Delta T_{sat}^{\,0.24} \Delta P_{sat}^{\,0.75} \tag{27}$$

where Re_{tp} is the two-phase Reynolds number expressed by:

$$\mathrm{Re}_{tp} = F^{1.25}\,\frac{G(1-x)D}{\mu_L} \tag{28}$$

$$\Delta T_{sat} = T_w - T_{sat} \text{ And } \Delta P_{sat} = P_{sat}(T_w) - P_{sat}(T_{sat})$$

The vapor generation rate is given by the following expression:

$$\Gamma_G = -\Gamma_L = \frac{q_e}{h_{fg} + Cp_L.\Delta T_{sat}} \tag{29}$$

3 Numerical Resolutions

Equations (2-6), which govern the evaporation of refrigerant flowing in the vertical tube, have five unknown parameters, namely α, u_L, u_G, P, and H_L. To solve this set of equations numerically, the tube was divided into infinitesimal sections. The heat flux, q_w, and the following inlet operating conditions for the refrigerant were considered:

– Inlet saturation pressure or inlet mixture temperature;

- Mixture mass flow rate;.
- Inlet flow quality.

The mixture is assumed to be saturated in inlet of bubble pump tube. The correlation between P-T-X, for the liquid phases, is given by Bourseau and Bugarel [33]. The density of the liquid mixture is calculated according to Tiliner-Roth and Friend [34].

H_{L0}, enthalpy of mixed liquid phase is given by Pátek and Klomfar [35]. The vapor density and the enthalpy are only depended on the pressure.

$$\rho_G = \rho_{G,\,sat}\,(P).$$

$$H_G = h_{G,\,sat}\,(P).$$

The equations were solved using the fourth order Runge-Kutta method at operating condition shown in table 1. Flow patterns were predicted by establishing the void fraction profiles along the tube length and the liquid velocity versus vapor velocity curves.

4 Model Validations

The calculated values of void fraction versus vapor quality using the two fluid model were compared with those obtained from the homogeneous model, Rouhani and Axelsson's correlation [36], and Zivi's correlation [37] (see Annex).

From this Fig. 1 we observe that the numerical values achieved in the present work show similar trend to the results of other models. For void fractions lower than 0.6 there is a great similarity between the calculated values using Rouhani and Axelsson's correlation and our results, being the absolute deviation between 1.3 and 8.0 %. For void fractions above 0.6, the absolute deviation is larger and can reach 17.0 %. Regarding the Zivi's model, which is applicable for annular flow regime ($\alpha > 0.8$), it gives values very close to our simulation results. The absolute deviation of this model does not exceed 5.5% and decrease to 0.37%. However, the difference between the values from the homogenous model and our numerical results is significant, being the deviation higher for the bubbly flow regime, for which the velocity deviation can reach

80 %. This deviation decreases for slug flow regime but is still important, while for the annular flow regime it decreases up to 20%.

5 Results and Discussion

5.1 Void Fraction Profiles. In the present study, the bubble pump was a vertical uniformly heated tube with an ammonia-water mixture. The void fraction profiles simulated for different tube diameters and different heat fluxes are shown in Fig.2-4. For all the curves, the void fraction increases at first with length and then becomes constant. This is because the amount of vapor generated increases when the heat flux increases along the tube.

Fig. 2 shows that the zone length for which the void fraction reaches its maximum value is as much significant as tube diameter is larger. This behavior is not clear for the strong heat fluxes (Fig. 3 and Fig. 4).

The effect that heat flux has on the void fraction is shown in Fig. 5. It can be seen that heat flux has a decreasing influence on the behavior of the void fraction when the value of heat flux increases. This decrease was probably due to the effect of flow regimes inside the tube pump.

5.2 Performance of the Bubble Pump. The variations in the liquid superficial velocity versus vapor superficial velocity are reported in Fig. 6-8. For a low heat flux, the curve slope is the same for all tube diameters (Fig. 6). However, as the tube diameter increases, the outlet liquid velocity decreases. This is because the volume weight increases with the tube diameter. The pumping ratio (U_L/U_G) is constant for

different tube diameters. In this heat flux range, then, the bubble pump performance is not influenced by the tube diameter.

When heat flux is increased to 15 $kW.m^{-2}$ (Fig. 7), the liquid velocity is maximum for small diameters (6 and 8 mm), but not for diameters of 10 and 12 mm. This can be explained by the effect of gravity on the pumping ratio.

For a higher heat flux (25 $kW.m^{-2}$), the liquid velocity value is maximum for all diameters at the same vapor velocity of 3 $m.s^{-1}$ (Fig. 8). This is due to the fact that the liquid velocity decreases when the void fraction is constant in the tube. The constant value of vapor velocity for which the liquid velocity starts to decrease is related to the maximum void fraction and the mass flow rate at a given heat input. This is because the mass flow rate is constant and the maximum void fraction value is independent of tube diameter (Fig. 4). For 25 $kW.m^{-2}$, the outlet pumping ratio increases as the diameter of the tube increases. The bubble pump performs better at greater tube diameters in these operating conditions.

5.3 Flow Patterns. In this section flow patterns are simulated by using the void fraction profiles and the liquid velocity versus vapor velocity curves.

5.3.1 Void Fraction Profiles. The critical void fractions for transition from bubbly to slug, slug to churn and churn to annular are, respectively, 0.3, 0.55 and 0.8.

Fig. 2-4 plots the limit flow patterns for different diameters and heat fluxes. The influence of the operating conditions on the lengths of different flow patterns can be observed. Tables 2-5 summarize the lengths of the zones occupied by the various flow patterns.

Tab. 2 shows the different regimes for 5 $kW.m^{-2}$ heat flux. It can be seen that the churn flow regime dominates the other regimes for all tube diameters except 6 mm. The length of the bubbly, slug and churn regime zones increases with the tube diameter, while the length of the annular regime zone decreases. This is because, at small diameters, flow patterns are controlled by surface tension; however, at higher tube diameters, the gravitational effect becomes more pronounced [7].

If the heat flux is increased to 10 $kW.m^{-2}$ (see Tab. 3-5), the annular and churn flow regimes become dominant followed by bubbly and slug regimes. For a heat flux higher than 15 $kW.m^{-2}$, the annular flow becomes the dominant regime. For example, for a tube diameter of 10 mm, the annular regime occupies 68% and 80% of the tube length for 15 and 25 $kW.m^{-2}$, respectively.

5.3.2 Liquid Velocity Versus Vapor Velocity Curves. In the same conditions the flow patterns can be deduced from liquid velocity versus vapor velocity curves. In bubbly flow regime, the vapor phase is in the form of bubbles distributed within the liquid continuum (i.e. the vapor velocity increases but the liquid velocity is constant). The flow pattern can reach the limit of the bubbly regime zone when the vapor phase elevates the liquid phase (i.e. liquid velocity does not have a constant value and the slug regime starts at this point).

The slug to churn transition was rather difficult to describe exactly, because of disagreement over the mechanisms responsible for triggering churn flow. For the transition from slug to churn flow in upward vertical tubes, there were four major mechanisms:

* Entrance effect [13, 38, 39],

* Wake effect [14],

* Bubble coalescence [16],

* Flooding [40, 41].

The liquid velocity versus vapor velocity curves do not make it possible to locate the slug-churn transition abscise along tube.

The transition of churn to annular flow regime was marked by a sharp change in slope, and was at approximately the same vapor velocity for all tube diameters. Churn-annular transition regimes are located at points at which the liquid velocity decreases and the vapor velocity increases. Fig. 8 plots the limits of the flow regimes.

Flow patterns are influenced by such parameters as the diameter of the boiling tube, heat flux and many others. The void fraction profile is the best method for determining the length of the zone occupied by each regime and defining the regime transition.

6. Conclusion

Flow patterns in the bubble pump were simulated using a two-fluid model. The following conclusions have been drawn:

- The behavior of the void fraction depends on the tube diameter and the heat flux. For a low heat flux ($q \leq 5 kW.m^{-2}$), the void fraction does not achieve its maximum value even at a high diameter. For 5 $kW.m^{-2}$, the flow patterns revealed by the void fraction profile show that bubbly, slug and churn flow regimes dominate annular flow at the highest tube diameter (for a tube diameter of 12 mm 30%, 24% and 46% of the tube's length is occupied by bubbly, slug and churn flow, respectively). When the tube diameter decreases, the length of annular flow increase from zero to 40% of the tube's length.

- For a high heat flux ($q \geq 15$ kW.m^{-2}), the void fraction is maximum for all tube diameters. The performance of the bubble pump increases with the tube diameter. The bubble pump functions in churn and annular flows at this heat flux.
- The flow patterns transition can be determined from the curves of liquid velocity versus vapor velocity obtained by numerical simulation. Using this method, the slug to churn transition is not defined.

Acknowledgements

This work is part of a R&D project funded by the Spanish Ministry of Science and Innovation within the Energy Program: ENE2006-15250.

Nomenclatures

A = tube cross-section area, m^2

B = defined in Eq. (13)

C = defined in Eq. (14)

C_1 = the portion of the heating surface not covered by bubbles

C_2 = coefficient related to the pumping factor

C' = virtual mass coefficient

C_D = drag coefficient for a single bubble

C_{FI} = interfacial friction factor

C_P = specific heat, J.kg^{-1}.C^{-1}

D = hydraulic diameter, m

F = convective boiling factor

f_{Lo} = fraction factor

F_{GI} = interfacial force for the vapor due to the mass exchange, $N.m^{-3}$

F_{LG} = interfacial force between the two phases, $N.m^{-3}$

F_{LI} = interfacial force for the liquid due to the mass, $N.m^{-3}$ exchange, $N.m^{-3}$

F_{WG} = force between the wall surface and the vapor, $N.m^{-3}$

F_{WL} = force between the wall surface and the liquid, $N.m^{-3}$

g = gravity acceleration, $m.s^{-1}$

G = mass flux flowing in the tube, $kg.m^{-}2.s^{-1}$

H = enthalpy, $J.kg^{-1}$

h = heat transfer coefficient, $Wm^{-2}.K^{-1}$

h_{fg} = evaporation heat from the liquid to the vapor, $J.kg^{-1}$

L = length, m

n = Blasuis constant

P = pressure, Pa

P_h = heating perimeter of the channel, m

Pr = Prandlt number

q_v = heat flux component for generating the vapor on the wall surface, $W.m^{-2}$

q = total wall heat flux, $W.m^{-2}$

R_B = bubble radius, m

Re_B = bubble Reynolds number

S = suppression of nucleate boiling factor

T = temperature, K

u = velocity, $m.s^{-1}$

x = vapor quality

Xtt = Lockhart-Martenelli parameter

Y = defined in Eq. (11)

z = axial location along the flow direction, m

Greek symbols

α = void fraction

μ = dynamic viscosity, Pa.s

ρ = density, $kg.m^{-3}$

σ = surface tension, $N.m^{-1}$

Γ = vapor or liquid generation rate per unit mixture volume, $kg.m^{-3}.s^{-1}$

η = phase distribution parameter,

ΔP = pressure drop, Pa

Indice

L = liquid

f = Fluid

Lo = liquid only

Go = vapor only

B = bubble

H = hydraulic

L = liquid

In = inlet

G, g = vapor

OSV = onset of significant void

sat = saturation condition

w = wall

CV = convective

sp = single phase

tp = tow phase

nb = nucleate boiling

npb = nucleate pool boiling

Annex: Void Fraction Correlations

- Homogenous model

$$\alpha = \frac{1}{1+\frac{\rho_G}{\rho_L}\left(\frac{1-x}{x}\right)}$$

- Rouhani and Axelsson drift flow model

$$\alpha = \frac{x}{\rho_G}\left\{\left(1+0.12(1-x)\left(\frac{gD\rho_L^{\,2}}{G_o^{\,2}}\right)^{0.25}\right)\left(\frac{x}{\rho_G}+\frac{1-x}{\rho_L}\right)+\frac{1.18}{G_o}\times\left[\frac{g\sigma(\rho_L-\rho_G)}{\rho_L^2}\right]^{0.25}(1-x)\right\}^{-1}$$

- Zivi model

$$\alpha = \frac{1}{1+\left(\frac{\rho_G}{\rho_L}\right)^{0.67}\left(\frac{1-x}{x}\right)}$$

References

[1] Benhmidene, A., Chaouachi, B., Gabsi, B., 2010, "A Review of Bubble Pump Technologies", J. App. Sc. 10, pp. 1806-1813.

[2] Nicklin, D. J., 1963, "The air-lift pump: theory and optimization", Transactions of the Institute of Chemical Engineers, **41**, pp 29-38.

[3] Lister, G. D. S., 1996, "The design and evaluation of a pumping system for a three fluid absorption refrigeration plant", B Sc Thesis, University of Cape Town.

[4] Pfaff, M., Saravanan, R., Maiya, M. P., and Srinivasa, M., 1998, "Studies on bubble pump for a water–lithium bromide vapor absorption refrigeration", Int. J. Refrigeration, **21**, pp 452- 462.

[5] Jeong, S., Lee, S. K., and Koo, K. K., 1998, "Pumping characteristics of a thermosyphon applied for absorption refrigerators with working pair of Li/Br", App. Therm. Engineering, **18**, pp 1309-1323.

[6] Delano, A. D., 1998, "Design analysis of the Einstein refrigeration cycle", PhD Dissertation, Georgia Institute of Technology.

[7] White, S. J., 2001, "Bubbles pump design and performance", M.Sc Thesis, Georgia Institute of Technology.

[8] [15] Koyfman, A., Jelinek, M., Levy, A., and Borde, I., 2003, "An Experimental Investigation of Bubble Pump Performance for Diffusion Absorption Refrigeration System With Organic Working Fluids". App. Ther. Engr., **23**G, pp. 1881–1894.

[9] Chisholm, D., 1983, "Two-Phase Flow in Pipelines and Heat Exchangers". Longman Inc., New York.

[10] Vicatos, G., and Bennett, A., 2007, "Multiple lift tube pumps boost refrigeration capacity in absorption plants," J. Energy S. Africa, **18**, pp 49-57

[11] Hewitt, G. F., and Wallis G.B., 1963, "Flooding and associated phenomena in falling film flow in a vertical tube," UKAEA Report No. AERE-R4022. HMSO, London.

[12] Radovich, N.A., and Moissis, R., 1962, "The transition from two-phase bubble flow to slug flow," MIT Report 7, pp 7673-22.

[13] Taitel, Y., Barnea, D., and Dukler, A.E., 1980, "Modeling flow pattern transitions for steady upward gas-liquid flow in vertical tubes," AIChE J., **22**, pp 345-354.

[14] Mishima, K., and Ishii, M., 1984, "Flow regime transitions criteria for upward two-phase flow in vertical tubes," Int. J. Heat Mass Transfer, **27**, pp 723-737.

[15] Chen, X., and Zhou, F., 1992, "Mechanism and criterion of upward gas liquid flow pattern transition," Transaction of Xian Jiaotong Uni, **26** (in Chinese).

[16] Brauner, N., and Barnea, D., 1986, "Slug-to-churn transition in upward gas-liquid flow," Chem. Eng. Sci., **41**, pp 159-163.

[17] Wallis, G. B., 1969, "One-dimensional two-phase flow," McGraw-Hill, New York, NY.

[18] Barnea, D. A., 1987, "Unified model for predicting flow pattern transitions for the whole range of pipe inclinations," Int. J. Multiphase Flow, **13**, pp 1-12.

[19] Haberstroh, R. E., and Griffith P., 1965, "Slug-annular two-phase flow regime transition," ASME 65-HT-52.

[20] Beattie, D. R. H., and Whalley, P. B., 1982, "A simple two-phase frictional pressure drop calculation method," Int J Multiphase Flow, **8**, pp 83-87.

[21] Zuber, N., and Findlay, J., 1965, "Average volumetric concentration in two-phase flow Systems," J. Heat Transfer **87**, pp 453-468.

[22] Levy, A., Koyfman, A., and Jelinek, M., 2006, "Flow Boiling of Organic Binary Mixtures", Int. J. Multiphase Flow, **32**, pp. 1300–1310.

[23] Yang, L., Zhang, C. L., 2005, "Two-fluid Model of Refrigerant Two-Phase Flow Through Short Tube Orifice", Int. J. Refrig., **28**, pp. 419-427.

[24] Seixlak, A. L., and Barbazelli, M. R., 2009, "Numerical Analysis of Refrigerant Flow Along Non-Adiabatic Capillary Tubes Using a Two-Fluid Model", App. Ther. Engr., **29**, pp. 523-531.

[25] Ishii, M., and Mishima, K,. 1984, "Two-fluid model and hydrodynamic constitutive relations," Nucl. Eng. Design, 82, pp 107-126.

[26] Richter, H. J., 1983, "Separated two-phase flow model: application to critical two phase flow," Int. J. Multiphase Flow, **9**, pp 511-530.

[27] Xu, J.L., Wong, T.N. and Huang, X.Y. 2006, "Two-fluid Modeling for Low-Pressure Subcooled Flow Boiling", Int. J. Heat Mass Transf., **49**, pp. 377–386.

[28] Chisholm, D., 1973, "Pressure gradient due to friction during the flow of evaporating two phase mixtures in smooth tubes and channel," Int. J. Heat and Mass transfer, **16**, pp 347-358.

[29] Baroczy, C. J., 1965, "A systematic correlation for two-phase pressure drop," Chem. Eng. Prog. Simp. Ser **62**, pp 232–249.

[30] Hainoun, A., Hicken, E., and Wolters, J., 1996, "Modeling of void formation in the subcooled boiling regime in the ATHLET code to simulate flow instability for research reactors," Nucl. Eng. Design, **16**, pp 7175-191.

[31] Chen, J. C., 1965, "Correlation for boiling heat transfer to saturated fluids in convective flow," Ind. Eng. Chem. Process Design and Development, **5**, pp 322-329.

[32] Celeta, G. P., Cumo, M., and Satero, T., 1993, "Forced convective boiling in binary mixtures," Int. J. heat and mass transfer, **36**, pp 3299-3309.

[33] Bourseau, P., and Bugarel, R., 1986, "Absorption–diffusion Machines; Comparison of the Performances of NH3–H2O and NH3– NaSCN", Int. J. Refrig., **9**, pp. 206–214.

[34] Tiliner-Roth, R., Friend, D. G., 1988, "Survey and Assessment of Available Measurements on Thermodynamic Properties of the Mixture {water + ammonia}", J. Phys. Chem. Ref. Data, 27, pp. 45-61.

[35] Pátek, J., and Klomfar, J., 1995, "Simple Functions for Fast Calculations of Selected Thermodynamic Properties of Ammonia–Water system", Int. J. Refrg., **18**, pp. 228–234.

[36] Rouhani, Z., and Axelsson, E., 1970, "Calculation of volume void fraction in the subcooled and quality region," Int J Heat Mass Transfer, **13**, pp 383–93.

[37] Zivi, S.M., 1964, "Estimation of steady state steam void fraction by means of principle of minimum entropy production," Trans. ASME. J. Heat Transfer, **86**, pp 247–252.

[38] Dukler, A. E., and Taitel, Y., 1986, "Flow pattern transitions in gas-liquid systems: measurement and modeling," Multiphase science and technology 2, Hemisphere, Washington DC 1986.

[39] Mao, Z. S. and, Dukler, A.E., 1993, "The myth of chum flow," Int. J. Multiphase Flow, **9**, pp 377-383.

[40] McQuillan, K. W., and Whalley, P. B., 1985, "Flow patterns in vertical two-phase flow," Int. J. Multiphase Flow, **11**, pp 161-175.

[41] Jayanti, S., and Hewitt, G. F., 1992, "Prediction of the slug-to-churn flow transition in vertical two-phase flow," Int. J. Multiphase Flow, **18**, pp 847-860.

List of Tables

Table 1. Operating conditions considered for simulation

Parameter	Values
Heat flux ($kW.m^{-2}$)	5 ; 10; 15 ; 20 ; 25
Tube diameter (mm)	6 ; 8 ; 10 ; 12
Mass flow rate ($kg.m^{-2}.s^{-1}$)	20
Tube length (m)	1.000
Ammonia concentration at the inlet	0.4
Inlet pressure pump (bar)	18

Table 2. Length of regime zone for different tube diameters at 5 $kW.m^{-2}$ of heat flux

Diameter (mm)	Zone regime length (m)			
	bubbly	Slug	churn	annular
6	0.15	0.12	0.29	0.44
8	0.2	0.16	0.40	0.24
10	0.24	0.22	0.56	0.08
12	0.3	0.24	0.46	0

Table 3. Length of regime zone for different tube diameters at 10 $kW.m^{-2}$ of heat flux

Diameter (mm)	Zone regime length (m)			
	bubbly	Slug	churn	annular
6	0.09	0.07	0.16	0.68
8	0.11	0.09	0.18	0.62
10	0.14	0.1	0.24	0.52
12	0.16	0.12	0.30	0.42

Table 4. Length of regime zone for different tube diameters at 15 $kW.m^{-2}$ of heat flux

Diameter (mm)	Zone regime length (m)			
	bubbly	Slug	churn	annular
6	0.05	0.05	0.1	0.8
8	0.07	0.06	0.12	0.75
10	0.09	0.07	0.16	0.68
12	0.11	0.09	0.18	0.62

Table 5. Length of regime zone for different tube diameters at 25 $kW.m^{-2}$ of heat flux

Diameter (mm)	Zone regime length (m)			
	bubbly	Slug	churn	annular
6	0.03	0.03	0.06	0.88
8	0.04	0.04	0.08	0.84
10	0.05	0.04	0.10	0.81
12	0.07	0.05	0.12	0.76

Lists of Figures

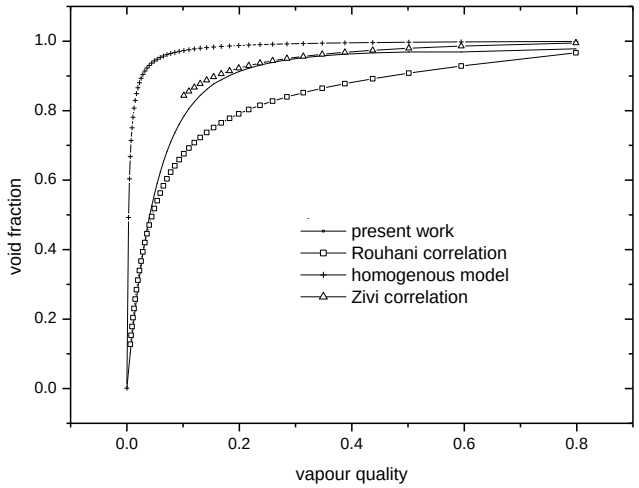

Fig. 1. Comparison of calculated void fraction values with other models

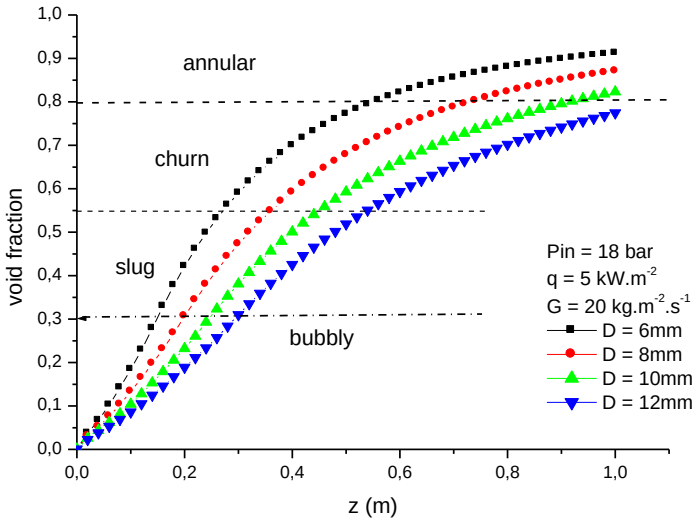

Fig. 2. Void fraction profile for different tube diameters (q = 5 W.m^{-2})

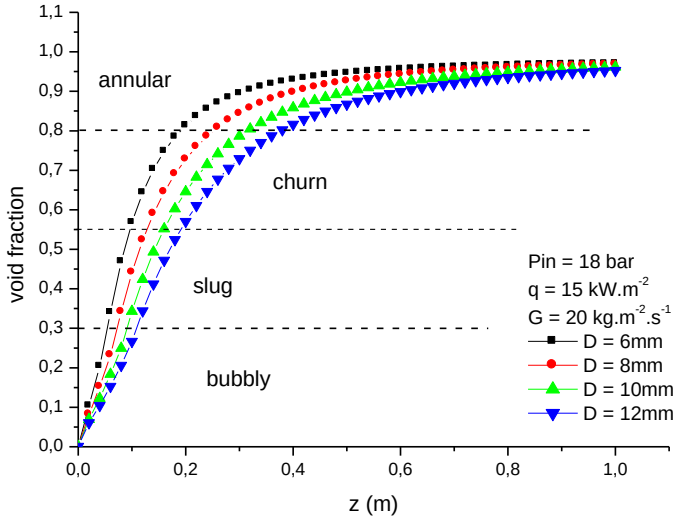

Fig. 3. Void fraction profile for different tube diameters (q = 15 W.m^{-2})

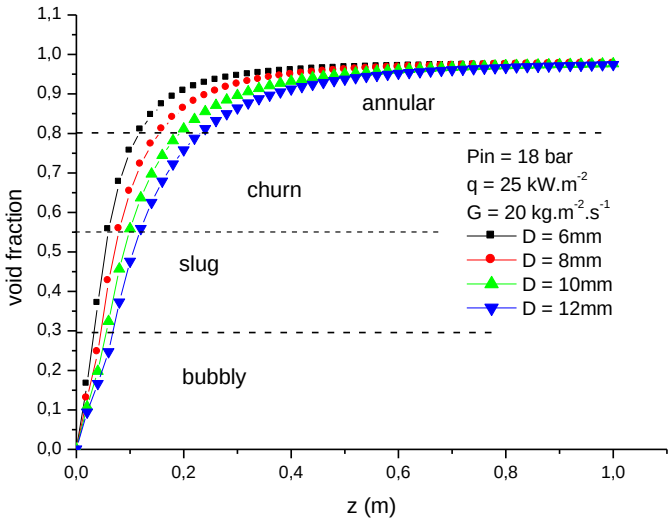

Fig. 4. Void fraction profile for different tube diameters (q = 25 W.m^{-2})

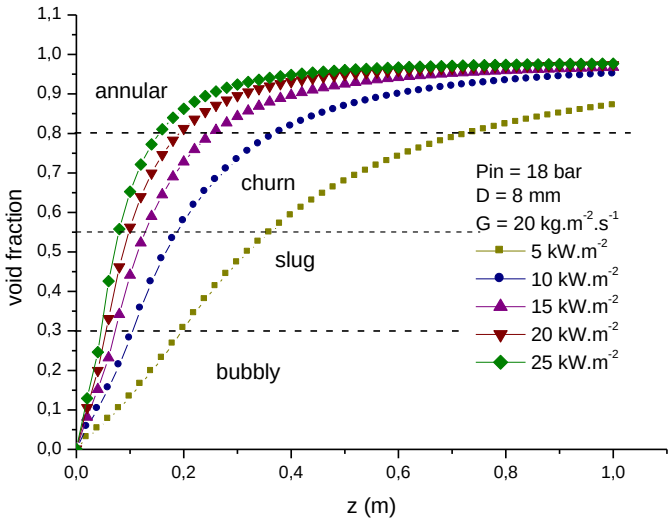

Fig. 5. Void fraction distribution for different heat fluxes

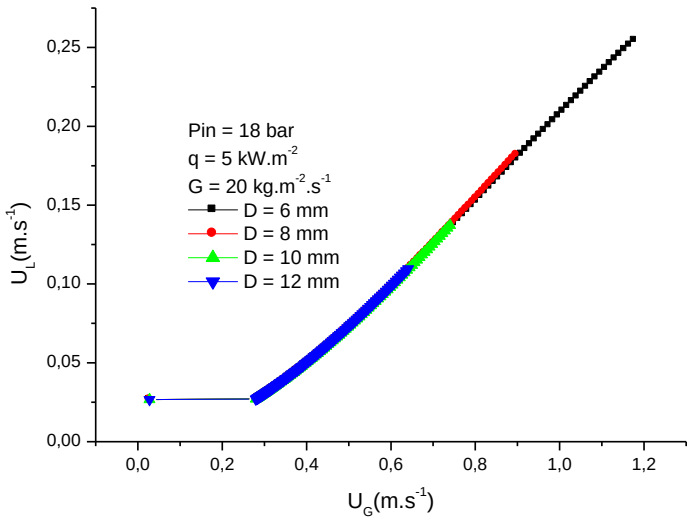

Fig. 6. Liquid velocity vs. vapor velocity for different tube diameters ($q = 5kW.m^{-2}$)

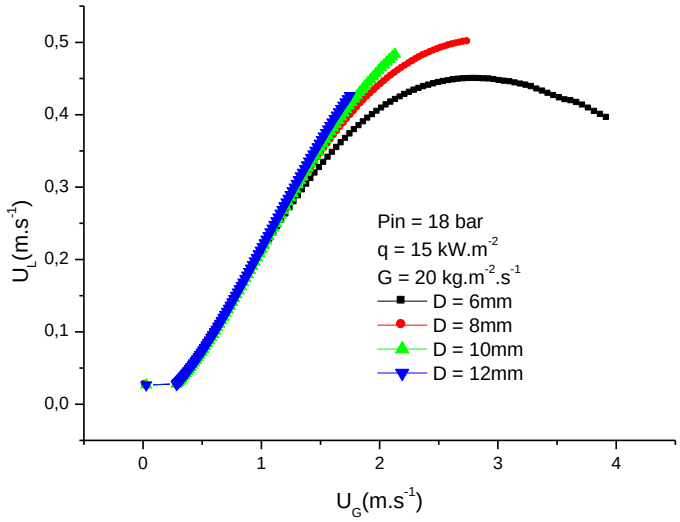

Fig. 7. Liquid velocity vs. vapor velocity for different tube diameters (q = 15kW.m^{-2})

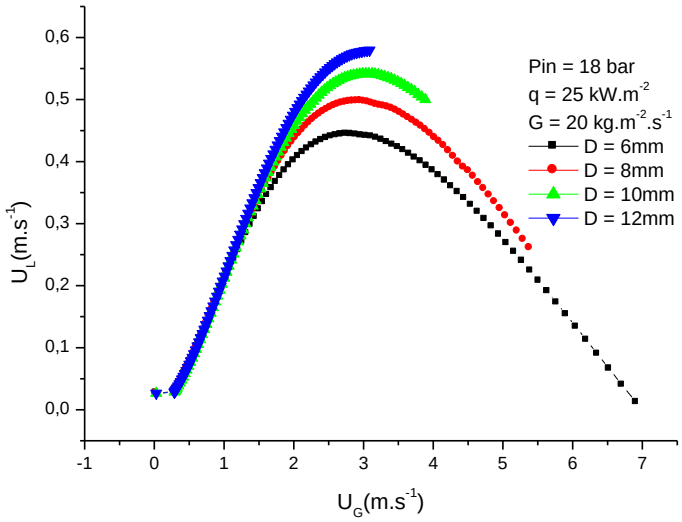

Fig. 8. Liquid velocity vs. vapor velocity for different tube diameters ($q = 25kW.m^{-2}$)

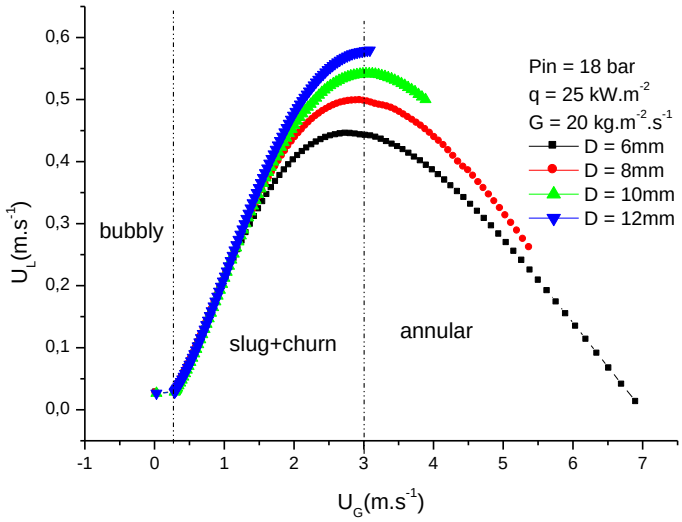

Fig. 9. Flow pattern map (q = 25kW.m^{-2})